



<http://dx.doi.org/10.5154/r.ctasci.2023.03.04>

English version

## Design of a monitoring control system for a Parabolic Trough Solar Concentrator (PTSC)

Eugueni Romantchik-Kriuchkova<sup>1</sup>; Carlos Martínez-Nicolas<sup>1\*</sup>;  
Gilberto de Jesús López-Canteñs<sup>1</sup>; Eduardo Ríos-Urban<sup>1</sup>

<sup>1</sup>Universidad Autónoma Chapingo, km 38.5 carretera México-Texcoco, Chapingo, Texcoco Edo. de México, C. P 56230. México.

### Article history:

Received: August 5, 2023

Accepted: December 12, 2023

### \*Corresponding author:

carlosmtz9904@gmail.com

### Abstract

The proper selection of a linear actuator for the position control system is crucial for the correct operation of a Parabolic Trough Solar Tracking Collector (PTSC). This study focused on determining the necessary actuator characteristics, such as size, force and displacement, and cost. An evaluation of the actuator options available in the market was carried out, considering their technical specifications. Through a comparative analysis of different PTSC positions, the optimal and efficient one for the system was selected, maximizing solar energy collection and minimizing costs. The PTSC position control system was designed and built. The optimum actuator position is vertical for the PTSC. The waiting times where the actuator takes to correct the PTSC position as a function of the solar trajectory varies from 10 to 100 seconds, giving an average of 25.4 seconds.

By means of a comparative analysis of different PTSC positions, the optimal and efficient one for the system was selected, maximizing solar energy collection and minimizing costs. The PTSC position control system was designed and built. The optimum actuator position is vertical for the PTSC. The dwell times where the actuator takes to correct the PTSC position based on the solar trajectory ranges from 10 to 100 seconds, yielding on average 25.4 seconds.

► **Keywords:** Solar thermal, PTSC, linear actuator, force, displacement.

### Introduction

Renewable energies are environmentally friendly sources of energy supply produced continuously and are non-exhaustible for human consumption. The adoption of renewable energy sources, such as solar energy, is essential to achieve sustainable development and reduce environmental impact (López et al., 2015).

Solar energy is an abundant, non-polluting energy source, and is available to a greater or lesser extent anywhere on the planet and can be collected and transformed into thermal or electrical energy (López-Cózar, 2006). Especially, solar

thermal energy takes advantage of the sun's radiation to heat a fluid, which is usually water or air (Martín-Domínguez and Alarcón-Herrera, 2004). EST (Solar Energy Transfer) can generate temperatures ranging from 45 °C to over 300 °C. Solar thermal collectors are devices that convert solar radiation into heat. These systems consist of a solar collector field with water or a combination of water and glycol circulating through it, a regulation system to control the heat requirements and the intensity of solar radiation, and a heating supply system (Ángel, 2013).

Solar collectors consist of parabolic reflectors, a structure with a metal support, receiver tube and independent solar

tracking system (Ramos, 2013). There are different types of tubes to be used, such as vacuum tubes that are resistant to extreme environmental conditions, which makes them ideal for industrial applications, or copper tubes, which stand out for optimizing the cost of their implementation (Aguamarket, 2022).

Parabolic trough solar tracking concentrators (PTSC) with tracking are a promising technology in the field of solar energy. These systems harness solar radiation by concentrating light onto a central receiver to generate heat or electricity. However, to ensure optimal PTSC performance, it is essential to select the right linear actuator that allows precise and controlled movement of the concentrator throughout the day (Osornio-Cárdenas et al., 2022).

Proper selection of the linear actuator for PTSC movement is essential to ensure optimal operation. There are different types of solar collectors, including stationary (such as flat plate collectors) and non-stationary (such as PTSCs) (Angel, 2013). The latter, by following the path of the sun, are more efficient in capturing direct radiation.

The thermal efficiency of a solar collector is the ratio between the useful energy added to the flow passing through it, in relation to the radiant energy reaching it from the sun. The difference between the two values is the heat losses that occur from the collector to its environment. It should be remembered that the collector temperature changes continuously, since water heats up as it passes through the device, it is understood that as the flow decreases and the outlet temperature increases, more losses are generated and efficiency decreases (Golato, 2008; Julián, 2022).

The use of solar tracking systems in PTSCs significantly increases the amount of radiation captured and the efficiency of the system compared to fixed systems (Estrada, 2016). In addition, the orientation of the PTSC, either East-West or North-South, can influence the amount of thermal energy produced at different times of the year.

The orientation of the solar concentrators can change according to the time of the year and the energy production objective, in order to increase the capture of solar rays for as long as possible, thus increasing solar incidence and, with it, the energy use. Solar tracking mechanisms can be used to orient the collectors towards the optimal position to capture the maximum solar radiation at any given time (Saldivar, 2022; Estrada, 2016).

For this project, it has been decided to work with the PTSC (Parabolic Trough Solar Collector) solar collector with tracking mounted with copper tubes. This type of collector uses parabolic mirrors to concentrate solar radiation onto a receiver tube, where heat is generated. Solar tracking increases the efficiency and the amount of solar

radiation captured by the collector. Linear actuators, the device responsible for the movement of the system, are mostly used for solar tracking (Firgelli, 2022).

The need to develop a linear actuator selection procedure for solar concentrating tracking systems (PTSC) is justified due to the scarce attention that has been paid to this specific aspect so far. This study focuses on determining the necessary characteristics of the actuator, such as size, force calculation and displacement, in order to verify in which positions the PTSC requires a higher and lower force based on the solar angle to establish restrictions in its displacement, to meet the system requirements and avoid selecting an inadequate actuator. An evaluation of the actuator options available in the market is performed and the best alternative that meets the established requirements is selected. It is important to ensure an effective and safe integration of the actuator in the system, verifying and validating its performance through tests and simulations. This procedure ensures optimal system performance by allowing precise and controlled movement of the solar concentrator, maximizing solar energy collection and minimizing costs.

## Materials and Methods

Our experimental site was Texcoco de Mora, Mexico (Renewable Energy Experimental Field DIMA "19.4912903, -98.8931657"), where all the necessary tests and measurements were carried out. The calculations of the diagrams in Table 1 were performed, taking into account the variation of the parameters from their minimum to maximum values of the solar tracking system, with specific intervals for each case of study to establish the required linear actuator.

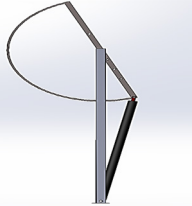
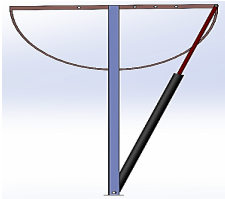
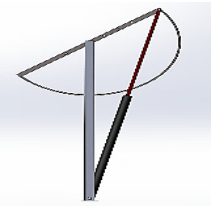
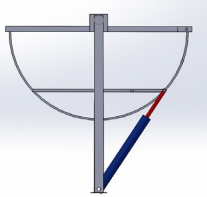
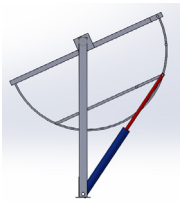
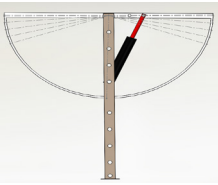
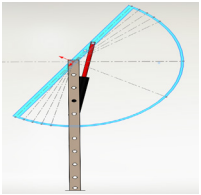
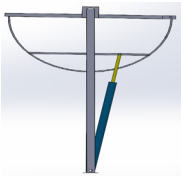
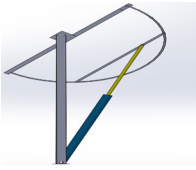
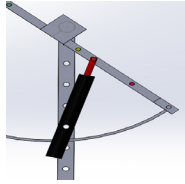
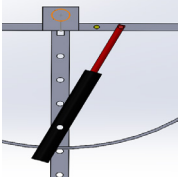
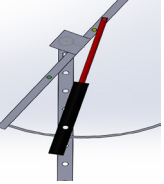
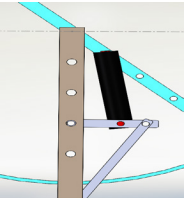
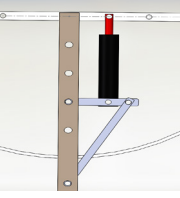
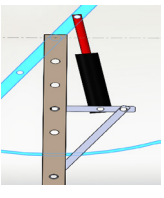
Measurements were carried out with precision and relevant data were collected during the PTSC testing with solar tracking. Each step of the process was recorded, ensuring traceability and accuracy in the results.

This methodological approach ensured reliable and representative data, which allowed a detailed analysis of the actuator and PTSC behaviors under different conditions. The integration of the experimental factors and the analysis of the results provided a solid basis for the selection and validation of the optimal linear actuator for the system.

### Linear actuator selection process

Proper design selection for actuator placement in relation to the PTSC is important to achieve accurate movement of the solar concentrator. There are several designs that can be considered, and each may have advantages and disadvantages depending on the specific needs of the system.

**Table 1. Diagrams of actuator position and PTSC in different positions.**  
**Cuadro 1. Esquemas de posición del actuador y CSCP en diferentes posiciones.**

No.	Minimum position Posición mínima	Horizontal position/ Posición horizontal	Maximum position/ Maxima posición
1. The actuator at its lower point is attached to the central frame, the upper attachment point of the actuator to the PTSC is located at a value to the radius.			
2. The actuator at its lower point is attached to the center frame, the upper attachment point of the actuator to the PTSC is located at the circumference.			
3. The actuator at its lower point is attached to the central frame, the upper attachment point of the actuator is strategically located on the horizontal axis.			
4. The actuator at its lower point is attached to the central frame, the upper attachment point is located on a horizontal axis.			
5. The actuator at its lower point is offset from the central frame, the upper attachment point of the actuator to the PTSC is located on the circumference.			
6. The actuator attachment point is located on the central frame and is located at the distance of its lower point, the upper attachment point of the actuator is located on the horizontal axis (Ramos, 2013).			
7. The actuator is aligned parallel to the vertical axis of the frame (the proposal), the upper attachment point of the actuator is located on the horizontal axis.			

**Note: Differences between diagrams exist in the connection points between actuator, concentrator and the base of each.**

**Nota: Las diferencias entre los esquemas existen en los puntos de conexiones entre actuador, concentrador y la base de cada uno.**

Several designs of different actuator placements in relation to the PTSC were analyzed looking for the optimal in displacement as shown in Table 1.

In Table 1, the “Minimum position means that the actuator is without elongation and the “Maximum position” means that the actuator is fully elongated.

In Section 7, the top attachment point of the actuator is strategically located on the horizontal axis of the PTSC. This position is crucial, as it ensures stable and balanced support of the actuator, allowing smooth and precise movement of the system. By placing the attachment point in this strategic position, an even distribution of forces is achieved and additional stresses that could affect the performance and durability of the PTSC are minimized. Furthermore, this arrangement facilitates easy access and maintenance of the actuator, which is essential for its proper operation over time.

**Estimation of required force for the actuator to be used**

According to the actuator placement diagrams (Table 1), calculations of the actuator forces required for PTSC movement are performed for different masses, radii and actuator stem displacements by varying the upper and lower attachment points. Analyzing the results, the actuator position with the lowest elongation and force is selected.

The methodology of force and displacement calculations is based on Figure 1 (a) and (b) where Figure 1 (a) shows the most common actuator position for all schemes (inclined)

and Figure 1 (b) vertically, which is the team’s proposal.

The following nomenclature is used in Figure 1:

Being  $\Delta L$  ne of the main parameters for the definition of the actuator to be implemented in the PTSC and which

$F_c = \gamma_{cylinder\ weight}(N)$

$F_a = \text{actuator force } (N)$

$g = \text{gravity } (m \cdot s^{-2})$

$l_a = \text{actuator length } (m)$

$l_h = \text{actuator fixation height } (m)$

$L_{oa} = \text{actuator fixation length } (m)$

$l_{CM} = \text{center - of - mass length } (m)$

$l_1 = \text{perpendicular distance to } F_c (m)$

$l_2 = \text{perpendicular distance to } F_a (m)$

$m = \text{cylinder mass } (kg)$

$\theta = \text{angle between } l_a \text{ and } l_{oa} (^{\circ})$

$\alpha = \text{angle of inclination of CSCP } (^{\circ})$

$r = \text{radius } (m)$

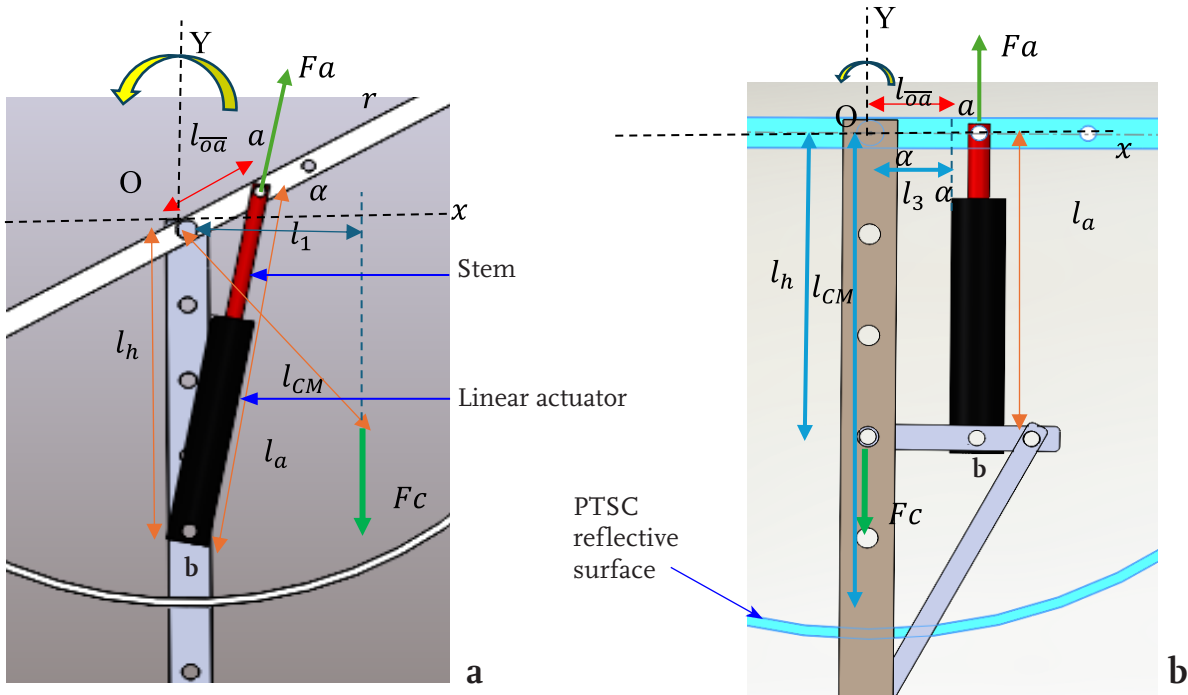


**Figure 1: Positioning of the actuator, (a)-tilted and (b)-vertical**

$a$  = actuator upper fixation point

$b$  = actuator lower fixation point

$O$  = center of rotation

$\Delta L$  = distance generated from minimum and maximum positions ( $m$ )

corresponds to the elongation generated by the actuator in the different positions from the minimum to the maximum of the PTSC, which is obtained by the law of cosines.

This projection is given by the actuator in relation to the distances attached to the PTSC and support.

To determine  $l_{a_{max}}$  and  $l_{a_{min}}$  the angles “ $a$ ” at the minimum

$$\Delta L_{max} = l_{a_{max}} - l_{a_{min}} \quad (1)$$

$$l_a = \sqrt{[(l_{oa})^2 + (l_h)^2 - 2(l_{oa})(l_h)(\cos(\alpha \pm 90))]} \quad (2)$$

and maximum position of the PTSC corresponding to the solar height in the morning and afternoon should be estimated, which are later addressed.

To find  $Fa$ , which is the second main parameter for actuator selection, a static equilibrium analysis of the PTSC under weight force and actuator force on point “O” Figure 1 ( $Fc$  and  $Fa$ ) is carried out. According to the following equation.

Or by substituting the parameters in Figure 1:

$$-(l_1 * Fc) + l_2 * Fa = 0 \quad (3)$$

Thus we obtain the value of  $Fa$ :

$$Fa = \frac{l_1 * Fc}{l_2} \quad (4)$$

Where  $l_1$  and  $l_2$  are completed in accordance with the following expressions

$$l_1 = l_{CM} * \text{sen}(\alpha) \quad (5)$$

$\alpha$  will depend on the position to be calculated and ranges from  $[0 \text{ a } 90]^\circ$  and from  $[0 \text{ a } -90]^\circ$

$$l_2 = l_{oa} * \text{sen}\theta \quad (6)$$

Where  $\theta$  is determined by the following equations

$$\cos\theta = \frac{(l_a)^2 + (l_{oa})^2 - (l_h)^2}{2(l_a)(l_{oa})} \quad (7)$$

$$\theta = \cos^{-1} \left[ \frac{(l_a)^2 + (l_{oa})^2 - (l_h)^2}{2(l_a)(l_{oa})} \right] \quad (8)$$

And finally, is determined by substituting in the previous expression

$$l_2 = l_{oa} * \text{sen} \left[ \cos^{-1} \left[ \frac{(l_a)^2 + (l_{oa})^2 - (l_h)^2}{2(l_a)(l_{oa})} \right] \right] \quad (9)$$

Using the values of we substitute them in the following equation:

$$Fa = m * \text{sen}(\alpha) * A \quad (10)$$

$$A = \frac{(l_{CM}) * 9.81}{l_{oa} * \text{sen} \left[ \cos^{-1} \left[ \frac{(l_a)^2 + (l_{oa})^2 - (l_h)^2}{2(l_a)(l_{oa})} \right] \right]} \quad (11)$$

$$F_k = \mu_k Fa \quad (12)$$

We consider the dynamic coefficient of friction for our PTSC.

Being  $l_{CM}$  the distance to the center of mass of the cylinder body which varies its dimension depending on the shape of the PTSC.

It is important to note that force  $Fa$  is influenced by both the angle  $a$  and the moving mass. Thus, it can be deduced that force  $Fa$  is mainly determined by the system mass and the distance to the actuator fixation points ( $a$ ). These two factors are essential to properly understand and calculate the force required for the correct operation of the PTSC.

### Solar angle calculation:

The calculation of the solar angle or solar height is relevant to be able to limit the tilt angle ( $\alpha$ ) of the PTSC from the effective sunshine hours.

Using as an example the specific area of interest Texcoco de Mora, Mexico, where the effective hours of sunlight in summer is from 8:00 to 17:00 hours.

To determine the angle  $\alpha$  during daylight hours the following formula is applied:

During the hours before noon.

$$\alpha = 90 - h \quad (13)$$

During the hours after noon.

$$\alpha = h - 90 \quad (14)$$

Where  $h$  is the solar height at a certain time of the day, and is determined by the following equation:

$$\text{Sen}(h) = [\cos(\lambda) * \cos(\delta) * \cos(\tau)] + [\text{sen}(\lambda) * \text{sen}(\delta)] \quad (15)$$

Where:  $\lambda$ - Latitude of location,  $\delta$  - Solar declination,  $\alpha$  - hour angle is presented in Table 2 (Franco, 2016),

Calculation of solar declination (Honsberg et al., 2019)

$$\delta = 23.45^\circ \left[ \text{sen} \left( 360 \left( \frac{284 + n}{365} \right) \right) \right] \quad (16)$$

Where n is the calendar day of the year.

The calculations and measurements made were for the area of Texcoco de Mora, México using the following data:

- Latitude  $\lambda=19^\circ 21'$
- Longitude  $x=99^\circ 12'$
- June 21 /  $n = 171$  (we choose the longest day of the year because it will be the day with the highest solar use in the area)

### Results and discussion

To obtain the solar declination values we substitute values in equation 16:

$$\delta = 23.45^\circ \left[ \text{sen} \left( 360 \left( \frac{284+171}{365} \right) \right) \right]$$

$$\delta = +23.444^\circ$$

Calculation of the hour angle to limit  $\alpha$  we have for the different angles, timetables shown in Table 2:

Table 2 Shows the solar height of each solar angle corresponding to each hour during the established day (21/06/2023) (El tiempo, 2021).

**Table 2: Solar height and energy output**

Time	Hour angle ( $\tau$ )	Solar height ( $h^\circ$ )	( $\alpha^\circ$ )	Power $W/m^2$
6:00	90	7	83	***
7:00	75	20	70	193
8:00	60	34	56	412
9:00	45	47	43	609
10:00	30	61	29	771
11:00	15	75	5	887
12:00	0	86	-4	949
13:00	-15	75	-15	953
14:00	-30	61	-29	896
15:00	-45	47	-43	780
16:00	-60	34	-56	614
17:00	-75	20	-70	432
18:00	-90	7	-83	215

**Note:** Source:(El tiempo, 2021)

Figure 2 shows the average energy distribution received on sunny days during the summer seasons in the area of interest specified above. According to the data for the year 2022, a maximum of  $8.47 \text{ kW}\cdot\text{hr}\cdot\text{m}^{-2}$  (Stackhouse, 2022).

It is thus deduced that solar height is found limiting  $\alpha$  for its efficient hours during the day at the minimum and maximum position of the angle  $\alpha$  making its displacement to be restricted in  $70^\circ$  in a positive movement and of  $-70$  in a negative movement to obtain the greatest solar utilization.

Fa are presented at different positions of  $\alpha$  for certain specific parameters of Table 3 from the formulas previously proposed, with  $\alpha$  being the inclination of the PTSC.

As seen in Figure 3, the specific measurements provided give a thrust force at the maximum position of  $1\,537.1 \text{ N}$  at  $70$  degrees in  $\alpha$ , however, for the given  $83$  degree position in relation to  $h$  the solar height gives us a force of  $6\,439.8 \text{ N}$  which is too high, so it is discussed whether it is really worth taking advantage of the  $200 \text{ W}\cdot\text{m}^{-2}$  produced in the last hour of the day, so we are forced to restrict in  $\alpha$  from  $-70^\circ$  in tension to  $70^\circ$  in thrust.

And as it can also be observed that  $\Delta L$  determined from the minimum to the maximum position, ranges from  $0$  a  $32 \text{ cm}$ , with this it is possible to deduce the necessary characteristics of the actuator being  $\Delta L$  the necessary measure required to be able to obtain the displacement (elongation) of the actuator for “Figure 1 (a)”.

#### Analyzing for “Figure 1 (a) and (b)”

Using the same values of Table 3 we obtain the different values of Fa in its negative and positive displacement:

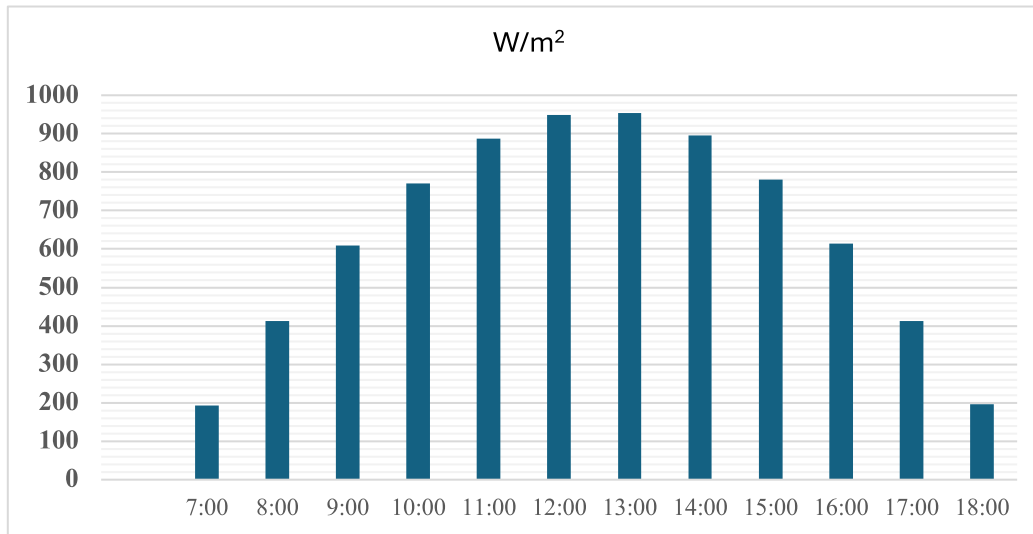


Figure 2. Energy power received on June 21, 2023, in Texcoco de Mora.

Table 3. Values used for Figure 1 (a)

Data	Units
PTSC, mass	20 kg
Radius	50 cm
$L_{oa}$	15 cm
$\Delta L$	28.0 cm

Note: Compiled by the author

Figure 3, the behavior of the force  $F_a$  in relation to the angle  $\alpha$  is presented visually, specifically for Figure 1 (a) and (b). This graphical representation allows to analyze and understand how the force  $F_a$  varies as the angles in Figure 1 (a) and (b) of the PTSC are modified. By looking at the plot in Figure 3, trends, patterns and points of

interest can be identified that help to better understand the relationship between the force  $F_a$  and the angle  $\alpha$ .

Figure 3 provides a comparative view of the behavior of the schemes in Figure 3 (a) and (b) according to the force  $F_a$  and angle  $\alpha$ . This graphical representation allows us to analyze and contrast how both the force  $F_a$  and angle  $\alpha$  vary in both PTSC schemes. By looking at the plot, similarities and differences in the patterns and trends of both lines can be identified, which provides valuable information about the relative behavior of Figure 4 (a) and (b) with respect to the relationship between the force  $F_a$  and angle  $\alpha$ .

Figure 4 shows how the variation  $\Delta L$  is linearly related to the angle  $\alpha$ .

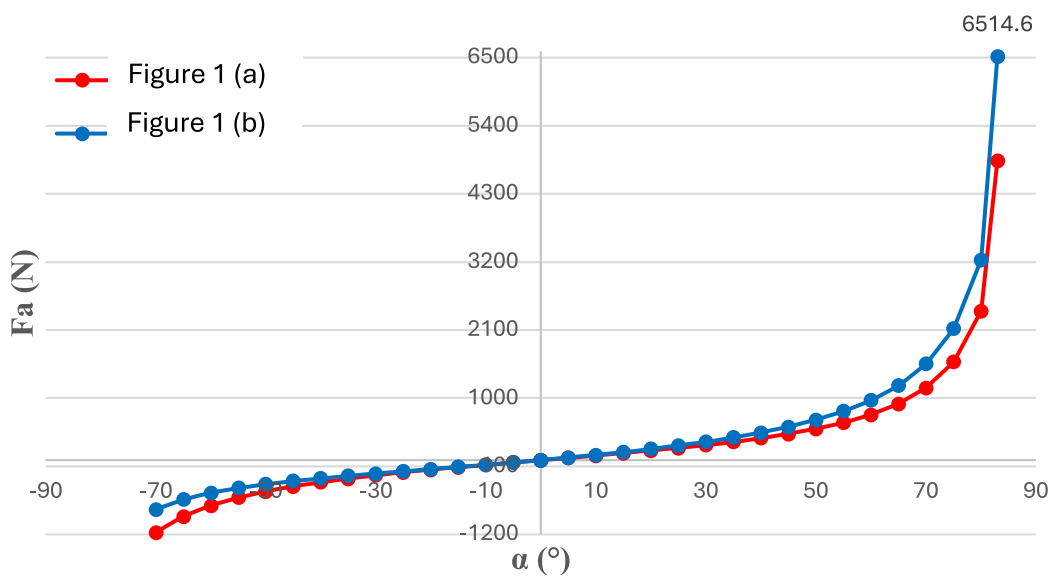


Figure 3. Comparison of forces for the schemes of Figure 5 (a) and (b)  $F_a$  compared to the variation of angle  $\alpha$  in its positive and negative position.

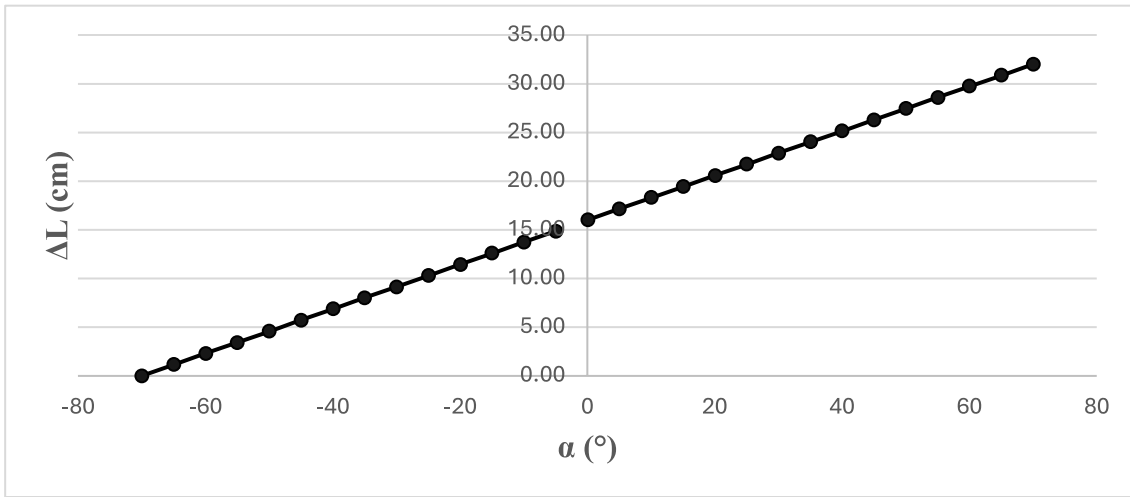


Figure 4. Length  $\Delta L$  changes proportionally as the angle “ $\alpha$ ” varies.

For Figure 1 (b) it can be analyzed that by moving the lower attachment point of the linear actuator perpendicularly to the attachment point “a”, the forces at the minimum and maximum position are proportional in their displacement  $\alpha$ , decreasing  $F_a$  by 25-40 % at its maximum position, implying that this position is the optimal position for the placement of the linear actuator since a smaller capacity actuator is needed to be able to generate the same expected displacement.

Figure 5 provides a clear visualization of how the force undergoes variations according to the distance  $L_{oa}$  from the center “O” of the PTSC system. As the  $L_{oa}$  position changes, a significant change in the magnitude of the force exerted on the system is observed. This graphical representation allows an immediate visual understanding of how the  $L_{oa}$  distance directly impacts the force applied to the PTSC system.

Figure 6, like Figure 5, allows observing the behavior of the force  $F_a$  regarding the center of the PTSC system with variation of  $L_{oa}$ . However, this graph clearly shows the

presence of symmetry in the negative and positive forces. The forces reach a maximum value in a specific position, as well as a minimum value in another position, but with opposite signs.

This obvious symmetry in the behavior of the forces provides an interesting perspective on the dynamics of the system. It shows how the location of the actuator for the PTSC system directly affects the resultant force.

Figure 7 examines the behavior of the length variation ( $\Delta L$ ) for the cases previously addressed in Figures 5 and 6. This graphical representation allows to analyze and compare how the length changes relative to the same PTSC schemes. By observing the graph, trends and differences in the  $\Delta L$  values for each case can be identified, which provides us with relevant information on how the length varies according with the schemes considered.

In the analysis performed, it can be argued that, given a specific value of  $L_{oa}$  for the schemes in Figure 7 (a) and (b), the change in  $\Delta L$  would be the same for both. This

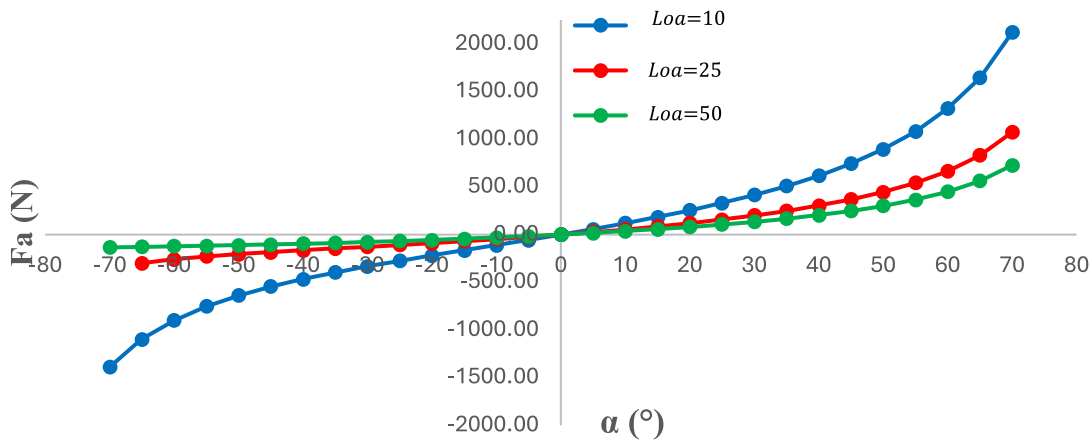


Figure 5.  $F_a$  required for the PTSC system of Figure 1 (a) with variation of  $L_{oa}$

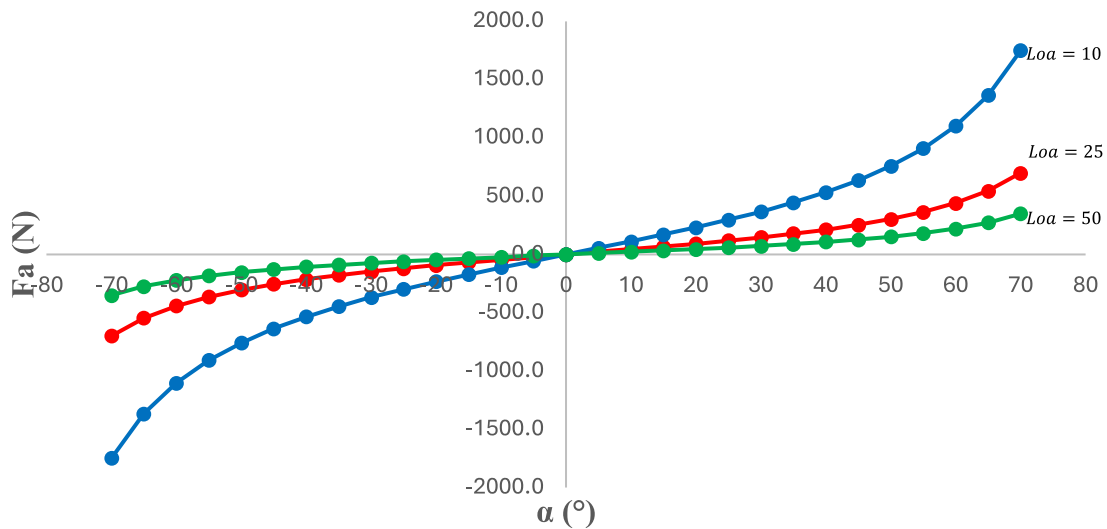


Figure 6. Fa required for the PTSC system in Figure 1 (b) with variation of  $L_{oa}$

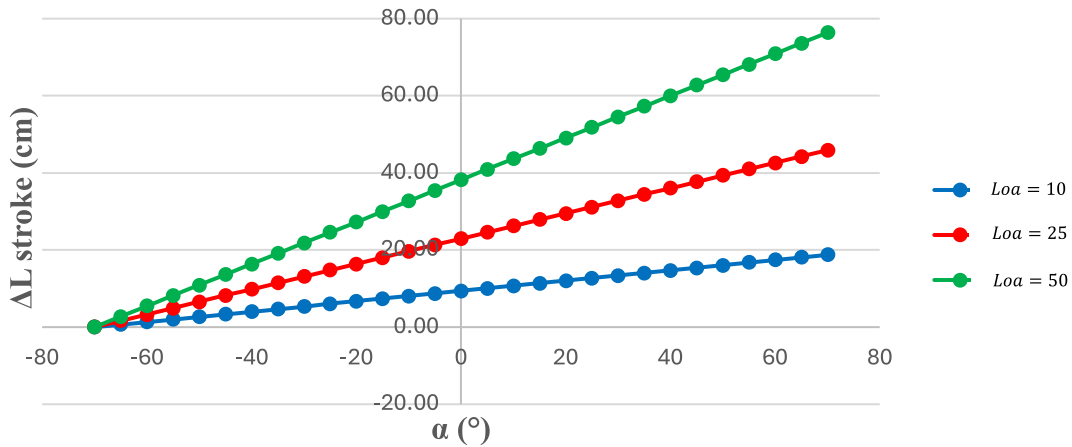


Figure 7. Behavior of  $\Delta L$  from the variation of  $L_{oa}$

is because it would represent the same stroke that the linear actuator would have to cover to meet the required displacement at angles of 70 and -70 degrees in  $\alpha$ . Consequently, the factor that is directly affected by the actuator’s lower attachment point would be  $F_a$  only, resulting in the behavior observed in Figures 7 and 8

These observations highlight how system design and configuration influence the relationship between  $\Delta L$ ,  $L_{oa}$  and  $F_a$ . By understanding and considering these variables, it is possible to analyze the behavior of the PTSC system more accurately.

Table 4 shows maximum  $F_a$  required for the correct displacement of the PTSC  $F_a$  for different radii and masses for “Figure 1 (a)”.

It can be seen how the force increases exponentially given a larger mass, for  $L_{oa} = 10$  cm.

For Table 5 changing ( $L_{oa} = 15$  cm) using different radii and masses the behavior of  $F_a$  is estimated as follows:

It can be seen how the force increases exponentially given a higher mass, but not more than the values presented in Table 4.

When analyzing the costs of the various actuators available, factors such as quality, reliability and cost-benefit ratio can be considered. By comparing actuator costs, the most suitable option for each specific  $L_{oa}$  and radius configuration in the PTSC system can be identified (Figure 1 (b)).

After performing calculations using equations (11) and input data such as radius (50-100, 10 cm), mass (10-60, 10 kg) and  $L_{oa}$  (10-100, 10 cm), the values of  $\Delta L$  and  $F_a$  were obtained in order to create a recommendation table for the different radii and masses that may be present. The

**Table 4. Fa with different radii and masses for “Figure 1 (a)”**

kg	Fa-r50 cm	Fa-r60 cm	Fa-r70 cm	Fa-r80 cm	Fa-r90 cm
10.0	1091.6 N	1309.9 N	1528.2 N	1746.5 N	1964.9 N
20.0	2183.2 N	2619.8 N	3056.5 N	3493.1 N	3929.7 N
30.0	3274.8 N	3929.7 N	4584.7 N	5239.6 N	5894.6 N
40.0	4366.4 N	5239.6 N	6112.9 N	6986.2 N	7859.5 N
50.0	5458.0 N	6549.5 N	7641.1 N	8732.7 N	9824.3 N
60.0	6549.5 N	7859.5 N	9169.4 N	10479.3 N	11789.2 N

Note: Compiled by the author

**Table 5. Comparison of Fa with different masses and radii for Figure 1 (b)**

kg	Fa-r50 cm	Fa-r60 cm	Fa-r70 cm	Fa-r80 cm	Fa-r90 cm
10.0	727.7 N	873.3 N	1018.8 N	1164.4 N	1309.9 N
20.0	1455.5 N	1746.5 N	2037.6 N	2328.7 N	2619.8 N
30.0	2183.2 N	2619.8 N	3056.5 N	3493.1 N	3929.7 N
40.0	2910.9 N	3493.1 N	4075.3 N	4657.5 N	5239.6 N
50.0	3638.6 N	4366.4 N	5094.1 N	5821.8 N	6549.5 N
60.0	4366.4 N	5239.6 N	6112.9 N	6986.2 N	7859.5 N

Note: Compiled by the author

optimal configuration results of the PTSC system parameters for Figure 1 (b) are presented in Table 6.

These results allow informed decisions and actions to be taken to ensure proper functionality of the PTSC system. By selecting the optimal parameter settings, optimum system performance can be achieved, considering both economics and functionality.

**Practical testing**

To verify and validate the collected data, a Parabolic Trough Solar Concentrator (PTSC) was designed and constructed at the specific location previously identified. The following instruments and tools were used to confirm the accuracy of the data collected:

- Radiometer and pyrometer: to measure solar radiation.
- Dynamometer: to measure force.
- Cell phone gyroscope: to determine the tilt angle.

The characteristics of the PTSC used in this validation are presented below, see Figure 8:

- Mass = 20 kg
- Radius = 45 cm
- $L_{oa}$  = 15 cm

<In the linear actuator implementation, both diagonal “D” and vertical “V” distributions were compared (Figure1)

**Table 6. Recommendation of actuators regarding Fa and ΔL.**

R (cm)	M (kg)	$L_{oa}$ (cm)	ΔL (cm)	Stroke (mm)	Fa (N)
50	10	10	19	200	875
60	20	20	37	400	1049
70	30	30	54	550	1224
80	40	40	68	700	1399
90	50	50	76	800	1574
100	60	60	80	800	1749
120	80	80	82	900	2099
140	100	100	83	900	2449
160	120	120	83	900	2799
180	140	140	84	1000	3148

Note: Compiled by the author



Figure 8. Implemented PTSC

- Current consumption: 3 A
- Power: 36 W
- Force: 150 kg · 1500 N<sup>-1</sup>
- Maximum piston stroke: 300 mm
- Total length with piston extended: 720 mm
- Moisture resistance: IP54
- Travel speed without load: 5 mm · s<sup>-1</sup>
- Operating temperature: -26 °C ~ + 65 °C
- Material: Aluminum alloy

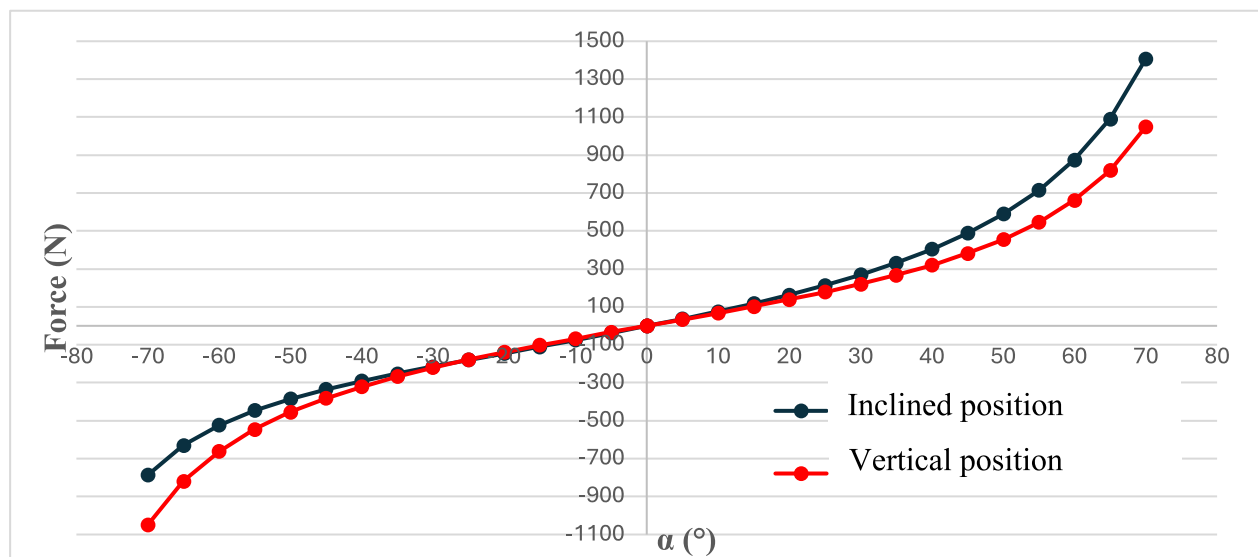


Figure 9.  $F_a$  in relation to  $\alpha$  for diagonal and vertical positioning.

(a) and (b) whose values of  $F_a$  regarding  $\alpha$  are shown in Figure 9 as follows:

Based on the values obtained, the decision was made to purchase a linear actuator that meets the displacements of  $\Delta L$  and  $F_a$  in the diagonal configuration of 1 407.5 N and in the vertical configuration of 1 049.5 N. The following are the characteristics of the selected linear actuator, which ensure optimum performance and the ability to meet the specific system requirements of the PTSC.

Specifications and characteristics of the purchased linear actuator:

- Model: R300X05
- Supply voltage: 12 V

- Weight: 1 240 g
- Dimensions: 420 x 73 mm (with piston retracted)

Figure 10. below shows the two configurations installed on the PTSC, the diagonal configuration corresponding to Figure 1 (a), the vertical configuration corresponding to Figure 1 (b).

Figure 11 presents the data collected throughout the day, which provide information about the system performance. These captured values represent key measurements that allow the performance of the solar tracking system to be evaluated and analyzed at different times of the day.

To incorporate the linear actuator to the PTSC, a circuit including sensors was designed and implemented to perform solar tracking throughout the day. This circuit had the following features:



Figure 10. Diagonal configuration corresponding to Figure 1 (a) vertical configuration corresponding to Figure 1 (b).



Figure 11. PTSC solar tracking during the day (8:00 a.m.-12:00 p.m.-06: p.m.)

- LDR sensors were used to detect the position and direction of the sun.
- It allows continuous tracking of the sun as it moves across the sky.
- Provides real-time feedback to adjust the position of the linear actuator.
- Integrated with the PTSC control system to ensure accurate tracking.
- Incorporates control algorithms to optimize solar tracking performance and efficiency.
- Allows customized settings and configurations according to the specific needs of the PTSC.
- Adapts to the specifications and technical requirements of the selected linear actuator and the PTSC in general.

The use of LDR sensors provides a simple and economical way to detect sunlight intensity. Proper placement of the

sensors at the top locations of the PTSC allowed for a balanced measurement of light intensity, which ensured efficient and accurate solar tracking.

Figure 12 presents the schematic implemented in the circuit to perform the solar tracking and illustrates how each individual component and the complete assembly was mounted on the PTSC to implement the solar tracking.

This setup allowed the correct implementation of solar tracking in the PTSC, ensuring optimal positioning of the concentrator in relation to the position of the sun throughout the day in real time.

With regard to the programming part, the code performs a solar tracking using four LDR (Light Dependent Resistors) sensors and an actuator that in summary are divided into the following points:

The pins corresponding to the four LDR sensors are assigned and the pins for the actuator control are defined.

In the setup function, the pins are initialized and a delay of 500 milliseconds is set.

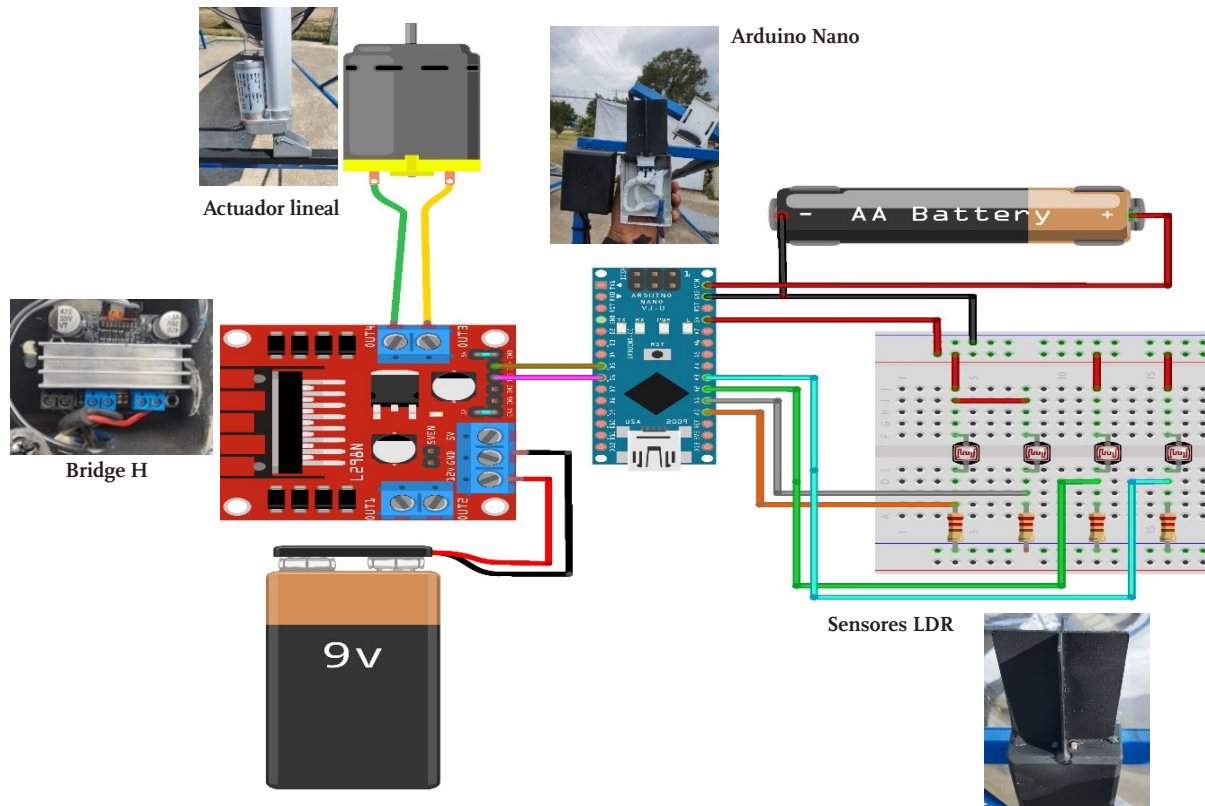


Figure 12. Circuit implemented for solar tracking and components.

In the main loop, the analog values of the LDRs are captured and the average of the upper and lower sensors is calculated.

The average of the sensor values is printed out via the serial port.

Based on the conditions, the actuator is activated in the appropriate direction to adjust the solar tracking.

If the average sensor values are equal, the actuator stops for 30 seconds.

If the sensor values are high (greater than 250), a specific movement of the actuator is performed which resets the actuator to its initial position to be ready for the next day and restart the solar tracking as shown in Figure 13.

The implemented code demonstrated the functionality of the system by making changes in the actuator direction according to the average sensor values. In addition, appropriate delays between actuator movements are included to ensure proper operation and avoid abrupt or unnecessary movements.

Figures 14, 15 and 16 present the results of the experiment corresponding to the day 08/07/23.



Figure 13. PTSC in its initial position in the mornings.

Figure 14 shows the waiting times where the actuator takes to correct the PTSC position according to the solar trajectory. The waiting time varies from 10 to 100 seconds, giving an average of 25.4 seconds.

For example, for 1 hour 20 min from 11:00 to 12:20 the actuator performed 152 movements, moving 53.3 mm or rotating PTSC by 20.8 degrees with the speed  $5 \text{ mm} \cdot \text{s}^{-1}$ .

In an action of 0.07 s duration with a wait of 31.5 s on average a displacement of 0.35 mm or a rotation of 0.13 degrees of the PTSC.

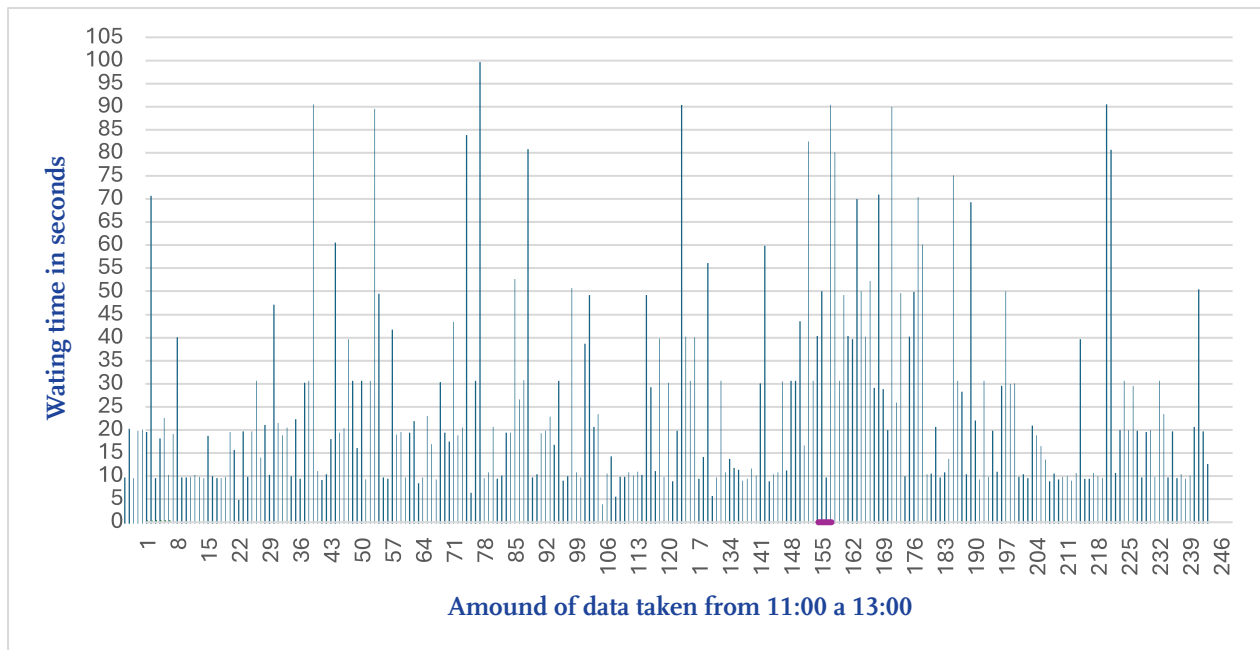


Figure 14. Actuator action waiting time.

Figure 15 shows the results obtained for the PTSC rotation from 8:00 to 16:00 from 66 degrees positive to -49 degrees with the average speed of 0.26 degrees per minute.

Figure 16 represents the room, inlet and outlet characteristic temperatures of the PTSC and the water heating temperature during the passage through the pipe with mass flow of 13.2 L·h<sup>-1</sup>, obtaining a maximum temperature of 52.1 °C at 13:50, with a maximum difference of 18 °C regarding the inlet temperature with a room temperature of 25 °C.

### Conclusions

The implementation of a PTSC scheme for mathematical analysis has provided a better understanding of the main parameters of the system's motion mechanism. This has facilitated the development to relate, calculate and analyze the forces and displacements of the PTSC, which is essential for the selection and proper sizing of the linear actuator.

An analysis of the relationship between the angles and the motion generated in the PTSC has provided infor-

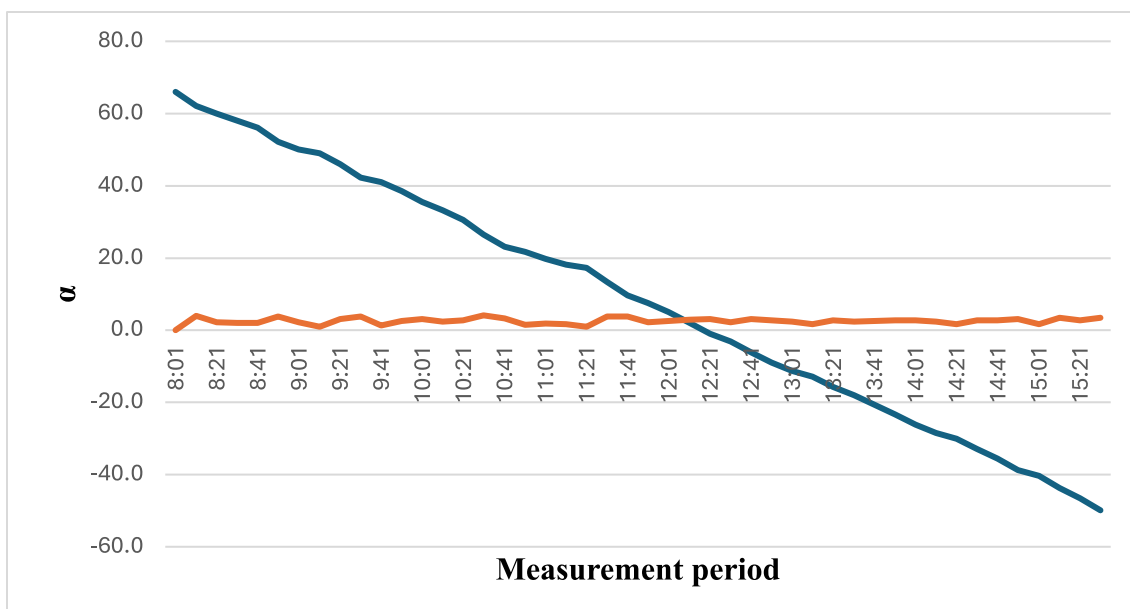


Figure 15. Measurement of angle  $\alpha$  during the day.

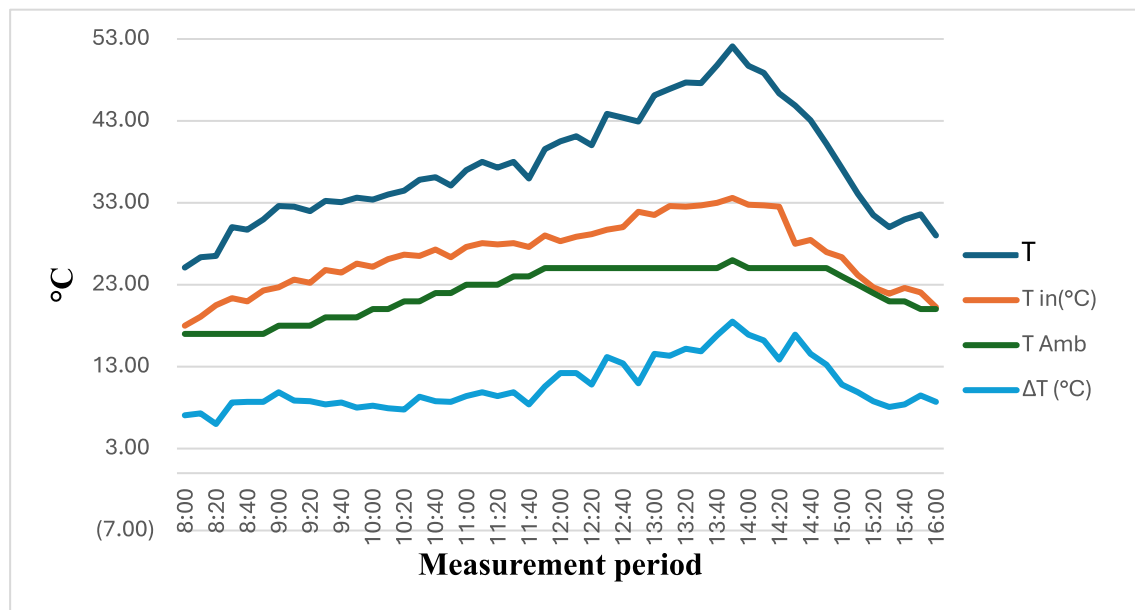


Figure 16. Daytime temperature measurement with solar tracking implemented.

mation to determine the required range of motion of the linear actuator.

Determining the actuator force at different positions of the PTSC has identified the critical points where a higher load capacity of the actuator is required. This is essential to ensure safe and reliable operation of the system, avoiding situations of overload or lack of force at key moments.

The analysis of the attachment distances and their impact on the actuator force in different positions has revealed the importance of a correct location and attachment of the actuator to the PTSC. A relationship of the actuator force according to the actuator attachment distance to the PTSC ( $L_{oa}$ ), the actuator attachment distance to the support ( $L_h$ ), radius and mass was found. These results are critical to ensure the structural stability and proper operation of the system during solar tracking.

An optimal position of the linear actuator was determined that is independent of the concentrator parameters which is vertical in its neutral position ensuring a minimum required actuator force thus reducing the cost of the actuator.

By analyzing and comparing the results obtained, the optimal linear actuator for the PTSC has been selected. This selection has been based on technical criteria, considering the specific system requirements and maximizing the solar tracking performance.

The code that was presented demonstrated an effective implementation of a solar tracking system using LDR

sensors and the linear actuator. The LDR sensors are strategically placed at the top positions on the PTSC to capture the incident light intensity. The actuator's movement direction was determined by reading and calculating the average sensor values, enabling precise adjustment of the PTSC towards the optimal solar tracking position.

The results of the 08/07/23 experiment demonstrate that the solar tracking system with the linear actuator on the PTSC is effective and efficient. The actuator succeeds in correcting the solar trajectory with average dwell times of 31.5 seconds. During an interval of 1 hour and 20 minutes, the PTSC performed 152 movements, moving 53.3 mm or rotating 20.8 degrees with speed of  $5 \text{ mm} \cdot \text{s}^{-1}$ . In addition, the tracking system achieved a movement range of 66 degrees positive to -49 degrees at an average speed of 0.26 degrees per minute. In terms of heat generation, the PTSC reached a maximum temperature of  $52.1 \text{ }^\circ\text{C}$ , with a difference of  $18 \text{ }^\circ\text{C}$  from the inlet temperature and a room temperature of  $25 \text{ }^\circ\text{C}$ . These results demonstrate the efficiency of the system.

## References

- Aguamarket. (2022). *Colector Solar de Polipropileno*. <https://www.aguamarket.com/productos/productos.asp?producto=7350>
- Ángel, B. C. (2013) "*Energía solar térmica*". <https://publications.iadb.org/publications/spanish/document/La-energ%C3%ADa-solar-t%C3%A9rmica-%C2%A1Deja-que-entre-el-sol!-Un-recurso-renovable-para-los-procesos-industriales.pdf>
- El tiempo. (2021). Tutiempo Network. <https://www.tutiempo.net/radiacion-solar/texcoco-de-mora.html>

- Estrada G. C. (2016). *Canal Parabólico y Fresnel*. concentracionsolar.org.mx. <https://concentracionsolar.org.mx/concentracion-solar/canal-parabolico-y-fresnel>
- Firgelli A. (2022). *¿Qué es un actuador lineal?* <https://www.firgelliauto.com/es/pages/what-is-a-linear-actuator>
- Franco A. (2016). *La ecuación del tiempo*. Dinámica Celeste. Retrieved July 2, 2023, from <http://www.sc.edu/es/sbweb/fisica3/celeste/tiempo/tiempo.html>
- Golato, M. A. (2008). *Metodología de cálculo de la eficiencia térmica de generadores de vapor*. [http://www.scielo.org.ar/scielo.php?script=sci\\_arttext&pid=S1851-30182008000200003](http://www.scielo.org.ar/scielo.php?script=sci_arttext&pid=S1851-30182008000200003)
- Honsberg, C., y Bowden, S. (2019). *Posición del sol*. Pveducation. <https://www.pveducation.org/es/fotovoltaica/2-propiedades-de-la-luz-del-sol/posicion-del-sol>
- Julián, C. (2022). *Fricción + Ejercicios Resueltos*. Fisimat | Blog de Física y Matemáticas. <https://www.fisimat.com.mx/friccion-ejercicios-resueltos/>
- López-Cózar, J. M. (2006). *Energía solar térmica*. Manual de energías renovables IDAE. Recuperado de [https://www.idae.es/sites/default/files/documentos/publicaciones\\_idae/documentos\\_10374\\_energia\\_solar\\_termica\\_06\\_8a90370e.pdf](https://www.idae.es/sites/default/files/documentos/publicaciones_idae/documentos_10374_energia_solar_termica_06_8a90370e.pdf)
- López, F. F., Ageitos, J. M., y Castiñeiras, J. P. (2015). *Energía Solar Térmica*. FACULTAD DE CIENCIAS DE LUGO, (p. 6-59).
- Martín-Domínguez, I. R., y Alarcón-Herrera, Ma. T. (2004). *Análisis paramétrico de colectores solares planos operando en serie*. <https://cimav.repositorioinstitucional.mx/jspui/bitstream/1004/1071/1/Publicacion%20Congreso%20Na1%20ANES%20Oaxaca%202004%20Colectores.pdf>
- Osornio-Cárdenas, J. I., Domínguez-Barreto, O., Miranda-Hernández, A., Reyes-Sandoval, F. A., y Vargas-Rosas, E. M. (2022). *Energía Solar Térmica*. TEPEXI Boletín Científico de la Escuela Superior Tepeji del Río, 9(18), 41-43.
- Ramos, C. (2013). *Concentrador solar de canal parabólico con seguimiento solar automático activo por servomotor y actuador mecánico* (Patent No. MEX/E/2000/063994). Instituto Mexicano de la Propiedad Industrial.
- Saldivar, T. (2022). *Caracterización y optimización del seguimiento solar de un concentrador solar de canal parabólico*. Tesis para obtener el grado académico de Maestro en Ciencias, Posgrado Interinstitucional de Ciencia y Tecnología.
- Stackhouse, P. (2022). *NASA POWER | Data Access Viewer*. <https://power.larc.nasa.gov/data-access-viewer/>